RSC Advances

REVIEW

View Article Online
View Journal | View Issue

Cite this: *RSC Adv.*, 2025, **15**, 45589

Recent progress in propane oxidative dehydrogenation: broad catalytic strategies and the role of vanadium

Erfan Nouri,[a] Zeynab Dabirifar,[b] Alireza Kardan [a] and Mojtaba Saei Moghaddam *[b]

Oxidative dehydrogenation of propane (ODHP) is emerging as an energy-efficient and environmentally favorable alternative to conventional steam cracking for propylene production. This review presents a comprehensive analysis of vanadium-based catalysts, emphasizing how their catalytic performance arises from the balance between active site structure, the physicochemical nature of the support, and the chosen synthesis method, which together control the dispersion and redox behavior of VO_x species. Thermodynamic and environmental aspects of ODHP are first outlined, followed by an in-depth discussion of active site chemistry, including the role of vanadium dispersion, oxidation state distribution, and coordination geometry in controlling C–H activation and product selectivity. Comparative evaluation of recent experimental data reveals that silica-based catalysts with isolated VO_4 species achieve high selectivity and stability, basicity-modified alumina systems suppress deep oxidation to attain selectivities above 94%, mixed-oxide supports balance redox activity with CO_x suppression, and carbon nanostructures or MOF-based supports enhance dispersion, thermal stability, and confinement effects. Recent advances demonstrate that promoter addition, tailored mesoporous supports, and controlled vanadium loading can shift the balance between isolated and polymeric VO_x species. This balance is critical in achieving high propylene selectivity while maintaining sufficient activity, optimizing the trade-off between activity and selectivity. Chemical looping ODHP is highlighted as a promising approach to further improve conversion efficiency and operational stability through controlled lattice oxygen delivery and facile catalyst regeneration. By integrating structural–functional relationships with process design considerations, this review provides a unified framework for developing next-generation vanadium-based ODHP catalysts, offering clear strategies for maximizing propylene yield, selectivity, and catalyst lifetime.

Received 25th August 2025
Accepted 14th October 2025

DOI: 10.1039/d5ra06338h

rsc.li/rsc-advances

1. Introduction

Propylene is a key building block in modern chemical manufacturing, used extensively in polypropylene, propylene oxide, acrylonitrile, and numerous other products.[1–4] Global production is expected to increase steadily in the coming years, driven by rising demand across the packaging, automotive, and consumer goods industries.[5] The conventional method of producing olefin includes steam cracking, catalytic dehydrogenation (CDH), and fluid catalytic cracking (FCC).[2,6,7] Familiar sources used in ethane steam cracking include naphtha and light petroleum gas (LPG). In these processes for producing olefins, the hydrocarbon compounds undergo homogeneous reactions to break down into smaller olefins. With FCC, primary feed materials typically include vacuum gas oil, leftover hydrocarbons from refining processes, and de-asphalted oil, all of which undergo conversion processes to produce valuable products like gasoline. Cracking reactions require a lot of heat because they absorb energy. To achieve this, reactor configurations capable of functioning under elevated temperatures are essential. Significant quantities of coke that are not wanted are produced, creating severe limitations for operations because of frequent halts in plant activity.[8,9]

CDH represents a cost-effective method for enhancing the quality of affordable saturated alkanes, like ethane and propane, by converting them into higher-value olefin feedstocks (for example, ethylene and propylene). The surge in shale gas production has reignited interest in developing cost-effective methods for transforming alkanes into olefins.[10,11] Converting alkanes to olefins through dehydrogenation is limited by thermodynamics. Currently, CDH is primarily utilized for propane and butane dehydrogenation. Various industrial-scale methods have been developed for propane dehydrogenation.[6,12] Some examples are OLEFLEX developed by UOP, CATOFIN by ABB

[a]*Department of Chemical Engineering, University of Guilan, Rasht, P. O. Box 41996-13776, Iran*

[b]*Department of Chemical Engineering, Faculty of Advanced Technologies, Quchan University of Technology, P. O. Box 9477177870, Quchan, Iran. E-mail: mojtabasaei@qiet.ac.ir*

Lummus, steam active reforming (STAR) manufactured by Phillips Petroleum, and fluidized bed dehydrogenation (FBD) by Snamprogetti. The reactor design, type of catalyst, and operating conditions differ among these technologies. Within these methods are distinct sections: one for dehydrogenation and another for catalyst regeneration.[13] Nevertheless, CDH demonstrates comparable restrictions to steam cracking and FCC. Specifically, they entail endothermic reactions and necessitate operating temperatures within 450–700 °C. At elevated temperatures, there is a possibility of coking and cracking, resulting in a restriction on the application of potentially beneficial catalysts like $Pt/Sn/Al_2O_3$ and Cr_2O_3/Al_2O_3. Current methods are inadequate to meet the growing needs of the olefin market because of these challenges, mainly since olefins are only produced as by-products in FCC.[6]

Therefore, in order to address the challenges linked with the dehydrogenation procedure, oxygen may be introduced into the reaction environment to enhance oxidative dehydrogenation (ODH).[14–17] Consequently, the process leads to an exothermic and irretrievable reaction, surpassing the thermodynamic constraints of dehydrogenation.[4,18] In this scenario, water emerges as a steady byproduct. The equilibrium constants observed in ODH are substantial and favorable, but they diminish as temperatures rise. Moreover, the existence of oxygen restricts coke formation, consequently prolonging the lifespan of the catalyst. This phenomenon seems particularly advantageous at the temperature of 650 °C, where ODH offers a distinct advantage over both non-oxidative and thermal catalytic dehydrogenation processes.[5,6]

Most ODH occurs in the temperature range of 400–700 °C with the incorporation of gaseous oxygen.[2,19] The process of catalytic ODH using oxygen in the gas phase presents obstacles, as it simultaneously introduces alkanes and gaseous oxygen. This leads to operating within the explosive zone. The oxygen required is expensive and energy-consuming, typically obtained through cryogenic air separation. In the presence of gaseous oxygen, ODH may facilitate the generation of electrophilic surface oxygen species like O^{2-} and O^{-}, which are created through the adsorption of gaseous oxygen. This process could potentially restrict the selectivity of the ODH reaction.[20,21] Furthermore, unwanted CO_x may also be generated through the direct combustion of alkanes or the extensive oxidation of the resulting olefins, leading to decreased olefin selectivity.[22]

Concerning homogeneous reactions of gas phase involving light alkane ODH selectivity, studies have demonstrated their significant impact at temperatures exceeding 600 °C. This process starts at the catalyst's surface by breaking the C–H bonds and creating radicals. These radicals can then be transformed into CO_2 within the gas phase, causing localized high-temperature areas and resulting in ethylene combustion losses in the gas phase.[23,24] In contrast, the oxidative dehydrogenation of lightweight alkane compounds does not share considerable drawbacks with the energy-consuming, coke-producing, and by-product-heavy endothermic pyrolysis of hydrocarbons. Primary obstacles in executing the oxidative dehydrogenation of small alkanes at the pilot and demonstration levels continue to include: (i) managing the exothermicity of the reaction, (ii) regulating sequential oxidation reactions. Inadequate regulation results in the generation of undesired side products, and (iii) ensuring that paraffin and oxygen blends are maintained within safe explosive thresholds to avoid runaway reactions.[25–27]

Although gas-phase molecular oxygen can potentially oxidize the carbon on the catalyst surface, it also reduces the selectivity towards olefins by promoting deep oxidation, leading to the formation of CO_x. Consequently, alternative methods that more effectively convert paraffin without gaseous oxygen are in great demand. Some researchers have suggested using mild oxidizing agents to prevent alkanes from being completely oxidized.[28,29] In order to tackle this problem, there is a deliberation on utilizing gentle oxidizing agents like nitrogen oxides. There is an expectation that using an appropriate catalyst may assist in surmounting the challenges posed by the CO_2 activation barrier in terms of thermodynamics and kinetics. In this context, the primary difficulty lies in activating a molecule of CO_2 for its use in ODH.[22]

Multiple researchers have conducted investigations into ethane and propane oxidative dehydrogenation in environments devoid of oxygen, as evidenced by the listed ref. 30–33. The exploration conducted by these scholars[34–36] focused on the oxidative dehydrogenation of light alkanes using only the oxygen present in the catalyst lattice. The prevention of extensive oxidation through catalyst lattice oxygen by ODH helps restrict CO_x emissions, resulting in an increased preference for olefins. In the present scenario, ODH in an oxygen-deprived environment is currently prioritizing the exploration of novel and enduring catalysts for ODH operations. Over the past two decades, a wide variety of catalytic systems have been explored for ODH, including transition-metal oxides, mixed oxides, carbon-based materials, and boron-containing catalysts. Within this diverse landscape, vanadium-based catalysts have consistently attracted attention because of their tunable redox properties, adaptability to various supports, and proven performance in both aerobic and chemical-looping configurations.[2,3,37] These catalysts are designed to release lattice oxygen efficiently at reduced temperatures (*e.g.*, 400–550 °C) while minimizing the generation of carbon oxides. Furthermore, the focus is on optimizing the reactor temperature control by leveraging the beneficial thermodynamics.[38,39]

This comprehensive review examines the crucial role of vanadium catalysts in ODH, a process of paramount importance for producing propylene, a vital feedstock in the chemical industry. The discussion delves into the thermodynamic and environmental considerations of various dehydrogenation methods, shedding light on the advantages and limitations of ODH. The review also investigates the active site in ODH, identifying the key factors influencing catalyst performance. A thorough analysis of industrial-scale propane dehydrogenation (PDH) processes, including emerging technologies, is presented, highlighting the current state and future directions of this field. Furthermore, the process of chemical looping ODH is explored, highlighting its potential for enhanced efficiency and reduced environmental impact. The review then comprehensively examines the diverse range of vanadium-based catalysts

employed in ODH, emphasizing their structure–activity relationships and performance characteristics. Finally, commercial strategies implemented in PDH are discussed, providing insights into the economic and technological aspects of this crucial industrial process.

2. The thermodynamic and environmental considerations of various dehydrogenation methods

Every dehydrogenation route presents distinct thermodynamic, economic, and environmental factors that influence catalyst development and the design of sustainable processes. The primary analysis here focuses on well-established procedures with abundant published data; however, no equivalent comprehensive studies exist for oxidative dehydrogenation. As a result, the environmental impacts of these newer reactions must currently be inferred from related systems. This section examines the thermodynamic and environmental aspects of each sub-process, citing relevant sources where available and highlighting factors likely to affect long-term viability when direct literature data are lacking.

2.1. Direct dehydrogenation

Direct dehydrogenation (DDH) represents an endothermic process with an equilibrium constraint seen when there are increased partial pressures of propane and reduced reaction temperatures ($\Delta H_{298}{}^{0}$ = 124 kJ mol^{-1}). Consequently, customary response temperatures in industrial DDH procedures range from 550 to 750 °C. An essential difficulty in the catalyst development for DDH involves the preference for producing coke alongside high propylene yield, with its formation believed to start through deep dehydrogenation. Fig. 1 depicts the common reaction routes seen in DDH. The generation of methane and ethene occurs through thermal and catalytic (gas-phase radical) cracking reactions. Ethene can subsequently undergo hydrogenation to become ethane. Additionally, propane can be subjected to hydrogenolysis, resulting in the production of ethane and methane.[3]

DDH has a significant atom economy of 95%, yielding only molecular hydrogen as a by-product, a valuable resource widely utilized as a carbon-neutral fuel. However, in reality, regular regeneration processes are essential to eliminate coke buildup, necessitating combustion to generate carbon dioxide. Therefore, the environmental consequences of this procedure will vary depending on the level of coke accumulation on the catalyst's surface. Propane, when used as a feedstock, is not harmful, as opposed to methanol, in the MTO process. Though propane's combustibility could pose safety hazards at a chemical facility, the same risk applies to all methods of propylene production.[3]

2.2. Oxidative dehydrogenation-O_2

ODH-O_2 is an exothermic process with a heat of formation of −117 kJ mol^{-1} (298 K, 1 atm), and the reaction is not constrained by thermodynamic equilibrium. Furthermore, coke production is significantly inhibited, with excessive oxidation being the primary alternative path. Fig. 2 illustrates the common reaction routes observed on ODH-O_2 catalysts. The principal issue is overoxidation, leading to the formation of by-products such as CO and CO_2. Cracking items are mentioned as secondary products, similar to the case of ODH-CO_2, where water is produced through oxidative dehydrogenation. Additionally, CO_2 may result from the direct combustion of propane.[40]

The incorporation of O_2 allows for the utilization of reduced operating temperatures, usually between 450 and 550 °C. This process is exothermic, resulting in lower energy expenses for maintaining the reaction temperature than ODH-CO_2 and DDH. Nevertheless, the efficiency of ODH-O_2 results in a 70% atom economy, producing H_2O rather than H_2 as a byproduct. Depending on the catalyst used, the production of CO_2 as a byproduct may occur, with the total amount of CO_2 generated

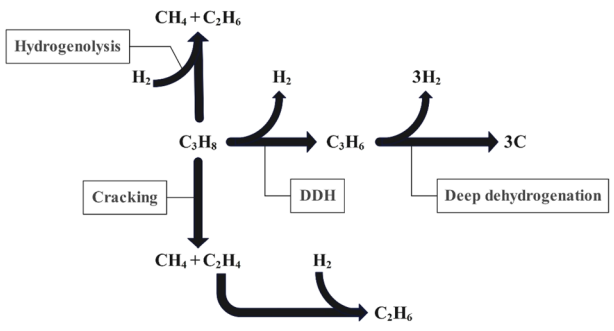

Fig. 1 Typical reaction pathways are often seen in the dehydrogenation of propane. In addition to the DDH process, there can also be cases of unwanted deep dehydrogenation causing coke formation, cracking, and hydrogenolysis. Adapted from ref. 3 with permission from the Royal Society of Chemistry, copyright 2021 (open access article under CC BY 3.0).

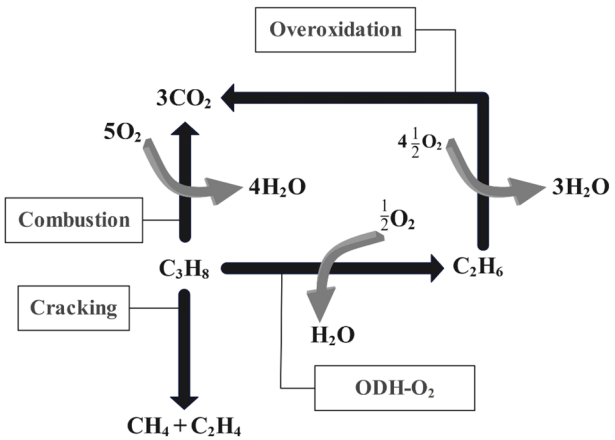

Fig. 2 Typical reaction routes seen in ODH-O_2 reactions. In addition to ODH-O_2, combustion, overoxidation, and cracking also occur. Adapted from ref. 3 with permission from the Royal Society of Chemistry, copyright 2021 (open access article under CC BY 3.0).

potentially resembling that of a DDH process. There will be a rise in energy usage linked to providing the oxidizing agent in adequate quality and quantity. When using air, it is necessary to separate nitrogen downstream, as this will increase energy consumption. The presence of O_2 and propane poses a heightened safety hazard, although the reactants and products are harmless. Even though a comprehensive environmental assessment is pending for the ODH-O_2 method in processing propane, it can be deduced that ODH-O_2 might offer comparable or even superior environmental benefits compared to DDH. It is primarily attributed to the anticipated reduced expenses in maintaining the reaction temperature. Yet, the comparison will heavily depend on the catalyst's effectiveness and structure. The financial implications of ODH-O_2 for producing propylene have not been examined. Nevertheless, extensive research has been conducted on the oxidation of C_2H_6, and there is existing documentation on this subject. In their study, Gaffney and Mason[3] compared the ODH-O_2 process of C_2H_6 with thermal cracking, showing that ODH-O_2 can reduce plant capital expenses and production costs. Due to the parallels observed in the decomposition and removal of hydrogen from ethane and propane, it can be inferred that the financial aspects linked to the ODH-O_2 process of propane are advantageous relative to steam cracking.[3]

2.3. Oxidative dehydrogenation-CO_2

In the ODH-CO_2 process, adding CO_2 leads to higher propylene yields by favorably shifting the thermodynamic equilibrium through the mildly endothermic reverse water–gas shift (RWGS) reaction. It makes ODH-CO_2 more endothermic than DDH, allowing it to be carried out at lower temperatures (450–600 °C). The reaction can proceed *via* a direct one-step ODH or through a combination of two parallel reactions: DDH and the RWGS, which may occur concurrently. However, competing reactions such as dry reforming of propane (DRP) and reverse Boudouard reaction with coke can impact propylene selectivity.[41] A study by Zangeneh *et al.*[42] analyzed the thermodynamics of ODH-CO_2, showing that dry reforming and coke formation side reactions can significantly affect propylene equilibrium conversion. Controlling these reactions kinetically is essential to prevent rapid catalyst deactivation and maximize propylene yield in the ODH-CO_2 process, where water is produced as a byproduct.

Utilizing ODH-CO_2 in a circular economy offers environmental benefits by consuming CO_2, contributing to combating climate change. Although producing water is not as preferred as producing hydrogen, the potential to decrease the carbon footprints of products and technologies by using CO_2 chemically is promising. By considering the sustainable use of CO formed in ODH-CO_2, such as in the water–gas shift reaction for hydrogen production or in syn-gas processes like methanol synthesis, a renewable carbon cycle can be established to avoid additional CO_2 emissions. This approach forms a crucial part of strategies to curb CO_2 emissions in the short and medium term, with carbon capture and storage technologies playing a vital role. Despite having a lower atom economy than other dehydrogenation reactions, ODH-CO_2 presents a respectable option, significantly when undesirable pathways are minimized through effective catalyst utilization.[43]

Each dehydrogenation reaction presents unique challenges and operating conditions based on their thermodynamics. For example, in the DDH reaction, coke formation is a major hurdle due to its thermodynamic favorability in conditions promoting high propane conversion. Similarly, in ODH-CO_2, dry reforming competes with the desired reaction, while ODH-O_2 may lead to overoxidation as CO_2 is the preferred product. To counteract these undesirable by-products, precise kinetic control is necessary. Catalyst design plays a crucial role in inhibiting or eliminating these side reactions, as will be explored in the following sections.

3. The active site in propane oxidative dehydrogenation

In the realm of catalysis, the fundamental elements typically found in a catalyst tailored for a specific purpose include the active ingredient, enhancer, and backing material.[44] The active sites, which are the primary catalytic hubs, are located within the active phase. Here, interactions occur involving adsorbates during reactions in the ODHP, which encompasses various catalyst types. Metal oxide-dependent catalysts, whether backed or unsupported, carbon-centered catalysts, metal catalysts that are supported, and boron-infused catalysts like hexagonal boron nitride are all part of the mix. The active centers accountable for the oxidative dehydrogenation of propane vary among different types of catalysts, with reactive oxygen species in various structural configurations commonly acknowledged as the key players on the catalyst surfaces.

In the upcoming section on tuning strategies, it will be highlighted that introducing heteroatoms, applying thermal and chemical processes to bulk catalysts, and selecting appropriate support materials can lead to considerable changes in the selectivity and reactivity of active oxygen species. Essentially, the variations in the selectivity, reactivity, and stability of active sites arise from alterations in geometric and electronic influences within the catalysts, which result from implementing suitable catalyst tuning approaches. For instance, doping with Ce or Ga can modify the electron density around vanadium, stabilizing isolated VO_4 units and thereby enhancing propylene selectivity, while thermal treatments can induce polymerization of VO_x species that increase activity but reduce selectivity. Events at the nanoscale significantly influence the reaction sites, ultimately determining the catalyst's overall catalytic properties. Furthermore, the presence of lattice strain and immediacy to surface imperfections like oxygen vacancies may impact the catalytic activity of active sites. Such vacancies not only provide pathways for oxygen mobility but also alter the redox balance of V^{5+}/V^{4+} species, directly affecting turnover rates. To directly investigate these impacts or evaluate their individual effects on catalytic performance, a comprehensive analysis is needed, utilizing sophisticated analytical methods, particularly *in situ* or *operando* spectroscopy and microscopy techniques in real-time or on-site conditions.[45–47]

Currently, researchers are studying catalysts that use metal oxides for ODHP, with the main active sites being the lattice oxygen species. The ODHP reaction is supported mainly by active sites through the Mars–van Krevelen (MvK) mechanism, which encompasses a series of oxidation–reduction processes on the surface of the metal oxide. Variations in catalytic properties can result from differences in the chemical surroundings[48] and positions[49] of lattice oxygen entities. One of the possible oxygen forms present on metal oxide catalyst surfaces is those that are captured as molecules (O_2), as well as neutral atoms (O), peroxide (O_2^{2-}), superoxide (O_2^-), oxygen radical (O^-), or ozonide (O_3^-).[50] The species that lack electrons (are electron-deficient) tend to have increased reactivity and decreased selectivity in chemical reactions with simple hydrocarbons under light influence like propane and ethane. The tendency in electrophilic nature is as follows: $O^- > O_3^- > O_2^{2-} > O_2^-$. Fig. 3 illustrates a diagram depicting the electrophilic and nucleophilic oxygen entities present on catalysts composed of metal (M) oxides. In ODHP, it is understood that lattice oxygen species carrying specific nucleophilic characteristics exhibit a high level of selectivity in producing propylene.[51] The principal factor influencing nucleophilic behavior is primarily the capacity of oxygen entities to provide electrons and the level of bonding strength in the metal–oxygen (M–O) interactions present within the functional zones. It is crucial to investigate the catalytic effects of different adsorbed oxygen molecules and the lattice oxygen species present on ODHP catalyst surfaces. The catalysts' composition–activity relationships can be clarified through carefully designed experiments that vary vanadium surface density, promoter addition, and support acidity/reducibility. Such studies reveal that isolated tetrahedral VO_4 species are typically associated with higher propylene selectivity, whereas polymeric VO_x domains and crystalline V_2O_5 favor higher activity but lead to over-oxidation and CO_x formation. These insights provide practical guidance for tuning vanadium loading and support interactions to balance activity and selectivity.[52,53]

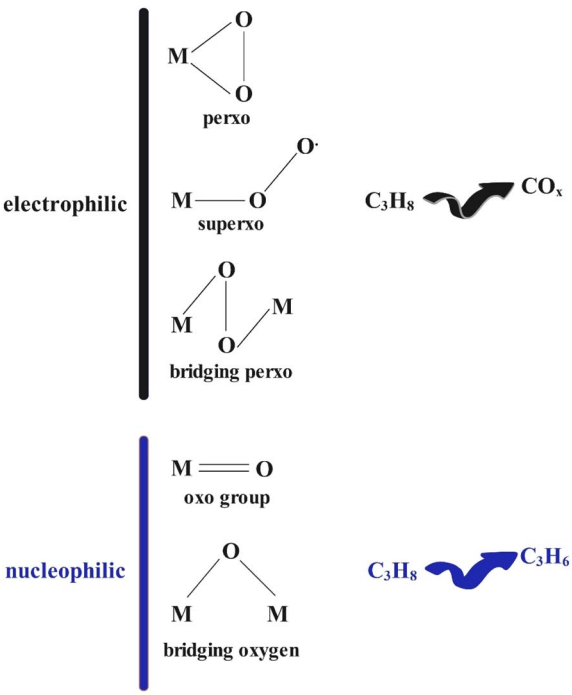

Fig. 3 Diagram illustration of oxygen compounds on catalysts made from metal oxides.

$$CH_3CH_2CH_3 + O^{2-} \rightarrow CH_3CHCH_3 + H_2O + 2e^- \quad (1)$$

$$O_2 + e^- \rightarrow O_2^- \quad (2)$$

$$O_2^- + e^- \rightarrow O_2^{2-} \rightarrow 2O^- \quad (3)$$

$$2O^- + 2e^- \rightarrow 2O^{2-} \quad (4)$$

In the process of ODHP, the reaction initiates by activating the propane molecule through the presence of surface-bound reactive oxygen species acting as the catalyst. Based on the characteristics of the active sites and the catalysts present, the C–H bond activation within the propane molecule can occur through either a single-electron transfer mechanism or a paired-electron transfer mechanism. The breaking of C–H bonds in propane molecules occurs through a single-electron process, leading to the formation of propyl radicals.[54,55] This homolytic bond cleavage contrasts with the heterolytic cleavage seen in the paired-electron mechanism.[54] However, most of the catalysts documented for the ODHP (particularly those based on metal oxides) aid in activating C–H bonds through nucleophilic oxygen species (characterized by strong primary sites) using the paired-electron process as shown in eqn (1). Following the activation of C–H bonds, an altered location emerges and requires restoration to facilitate the subsequent catalytic process. Eqn (2) through (4) demonstrate the activation of gaseous-phase oxygen to regenerate the nucleophilic lattice oxygen species at the reduced site, with each mole of oxygen requiring four electrons during the oxygen reduction process.[49]

A research conducted using density functional theory focused on Ti_2C MXenes with terminations, where a strong connection between hydrogen affinity and the activation of C–H bonds in propane was identified.[56] It is essential to mention that the current evaluation does not aim to delve deeply into the C–H activation mechanisms of the different catalysts utilized in ODHP. Typically, the initial C–H activation step is commonly considered to be the step that determines the overall rate.[57,58] Subsequently, the production of propylene or other unwanted products like CO_x is influenced by the specific interactions between the reaction sites and the generated intermediates. The effectiveness of a catalyst in ODHP lies in the capacity of its active sites to support the intermediates during catalysis and guide the reaction toward the intended outcome. Restoring the diminished functional sites plays a crucial role in the catalytic loop, significantly influencing the selectivity and activity of the ODHP procedure. The revival of the diminished area commences by capturing the oxidizing agent (CO_2, N_2O, O_2) from the gaseous stage, and its initiation at the area (eqn (2)–(4)). The type of oxidizing environment employed in the re-

oxidation process of the catalysts that have been reduced significantly influences the characteristics of the oxygen species present on the regenerated sites. An analysis conducted on the VO_x/MCM-41 catalyst using electron paramagnetic resonance (EPR) spectroscopy demonstrated that re-oxidation in a gas-phase oxygen environment leads to the production of more reactive electrophilic anionic oxygen radicals with reduced selectivity.[59] In the presence of N_2O gas, there was no observation of oxygen species that fully combust propylene molecules; instead, it is likely that diamagnetic nucleophilic species O^{2-} were produced.

Moreover, in catalysts that contain boron, active sites such as trigonal boron borosilicate zeolite,[60] armchair oxygen-terminated structures (>B–O–ON<) on h-BN,[61] imperfections on h-BN,[62] tricoordinated boroxol and hydroxylated linear structures of boron on B_2O_3/SBA-15,[63] as well as the edge-located hydroxyl group on BNOH,[64] have been identified as the key centers contributing to the propylene selectivity observed in ODHP. In the case of catalysts made of carbon, functional groups containing oxygen are predominantly the active sites responsible for carrying out oxidative dehydrogenation functions.[65,66] The oxygen clusters might be found at armchair or zigzag ends, and could be altered substantially by oxidizing conditions or exposure to acids and other substances like phosphates.

Regardless of the specific composition of the catalyst, be it based on metal oxides or carbon-based materials (carbocatalysts), those featuring nucleophilic oxygen groups consistently demonstrate a higher selectivity towards the desired product, even though they may exhibit a lower overall reactivity compared to their electrophilic counterparts. The most nucleophilic oxygen groups include quinone and diketone situated on zigzag and armchair edges in a range of oxygen functionalities, as discussed in ref. 67. The existence of imperfections on carbon-based catalysts like carbon nanotubes (CNT) may have a positive impact on the creation of ketonic carbonyl groups *via* oxo-functionalization, with the resulting sites displaying a high level of selectivity in ODHP.[68] Liu *et al.* found a strong correlation between the ODHP reaction rate and the quantity of carbonyl-quinone in hydrothermally-synthesized ordered mesoporous carbon catalysts, as detailed in their study.[69] Sun *et al.* conducted a study to explore how the addition of boron impacts nanodiamond during ODHP.[70]

The researchers found that with a moderate amount of boron added, there was a notable reduction in the creation of electrophilic oxygen sites that promote CO_x products. This outcome was realized as the dopant showed a preference for engaging with the existing surface imperfections of the nanodiamond catalyst. Nevertheless, an increase in dopant concentration resulted in the obstruction of the surface carbonyl groups, causing a shift to tetrahedrally coordinated boron and reducing propylene selectivity. The latest discovery reveals that active sites responsible for the oxidation of propane on graphitic carbon nitride (g-C_3N_4) are modified carbonyl groups situated at the edge, as confirmed by *in situ* diffuse reflectance Fourier transform infrared spectroscopy (DRIFTS).[71] It is essential to mention that the informative insights into the nature and behavior of active sites of mixed oxide catalysts for ODHP can be found in the review articles authored by Schlögl[72] and Védrine *et al.*[73] It is clear that when fresh catalysts are activated or reduced catalysts are re-oxidized, defects and various oxygen species like dissociatively adsorbed (O^-) and chemisorbed (O^{2-}) species may be present on catalytic surfaces. This factor has significantly added to the challenge of comprehending the distinctive characteristics of active sites in the majority of the ODHP catalysts that have been documented. Additionally, a notable distinction in the activation of the C–H bond between direct PDH and ODHP lies in the fact direct PDH proceeds mainly through homolytic cleavage, generating radical intermediates ($\cdot CH_2$–CH_3), whereas ODHP favors heterolytic cleavage, in which lattice oxygen withdraws a hydride to form surface hydroxyl groups and carbocations. This mechanistic difference explains why ODHP generally exhibits higher selectivity to propylene under suitable oxygen supply, while PDH is more prone to radical recombination leading to coke and by-products.[74] The latter process takes place on catalysts that are reduced and possess coordinatively unsaturated cations serving as active sites.[75–77] It indicates that an analysis can be conducted on a catalyst for both PDH and ODHP functions based on the type of catalytic evaluation process.[78] An improved way to accurately represent the inherent efficiency of active sites is with turnover frequency (TOF) rather than relying on traditional percentage conversion measures. The TOF metric assesses the efficiency of a catalyst relative to the number of estimated active sites and is therefore a valuable, though not definitive, descriptor for comparing catalysts in a given reaction. In VO_x-based systems, uncertainties in quantifying the exact number and nature of active sites (isolated *vs.* polymeric species, surface *vs.* bulk contributions) mean that TOF values should be interpreted cautiously and ideally complemented with other metrics such as conversion, selectivity, and stability.

4. Processes for PDH in industry and upcoming technologies

4.1. OLEFLEX process

The Honeywell UOP OLEFLEX technology, commercialized in 1990, converts propane to propylene *via* catalytic dehydrogenation in moving-bed reactors. OLEFLEX employs a Pt/Al_2O_3 catalyst with proprietary promoters, fully regenerable in continuous operation, enabling lower platinum loadings and high propylene selectivity.[79] The C_3 LPG feedstock is pretreated in a depropanizer to remove butane and heavier fractions. The overhead propane-rich stream enters the OLEFLEX reactor section, producing propylene of chemical or polymer grade and hydrogen-rich gas. Excess hydrogen can be used in a PSA unit or as a fuel. OLEFLEX plants are often integrated with downstream alkylation or isobutylene dimerization/hydrogenation (InAlk™) to produce high-octane fuels.[80]

4.2. CATOFIN process

The CATOFIN technology (ABB Lummus/Clariant) dehydrogenates C_3–C_5 alkanes using a fixed-bed CrO_x/Al_2O_3 catalyst

Table 1 Summary of major PDH technologies

Process	Catalyst	Reactor type	Temp (°C)	Conv. (%)	Sel. to propylene (%)	Regeneration mode	Key features/notes
OLEFLEX	Pt/Al_2O_3 (promoted)	Moving bed	550–600	~40–45	~88–90	Continuous moving bed	Widely used; regenerable Pt; integrated alkylation possible
CATOFIN	CrO_x/Al_2O_3 (>18 wt% Cr)	Fixed bed	~650	~43–45	>87	Cyclic air burn	HGM reduces CO_2; high Cr load
FBD-4	CrO_x/Al_2O_3 (+metal promoters)	Fluidized bed	~600–700	~45	~80	Continuous regeneration	Good heat transfer; Cr toxicity issue
STAR	Pt–Sn/Zn–Ca aluminate	Fixed bed	~580–620	~40–45	High (≈90)	Cyclic air burn	ODH integration shifts equilibrium; long life
Linde PDH	Pt–Sn	Multi-tubular fixed bed	550–650	~42–45	>90	Periodic regeneration	Isothermal; long catalyst life
ADHO	Non-noble MO_x	Circulating fluid bed	~600	~45	~80	Continuous regeneration	No feed pretreatment; eco-friendly catalyst
K-PROt	Non-precious, non-Cr	FCC-type riser	~600	~45	High	Continuous regeneration	Flexible integration; low cost
FCDh	K–Pt–Ga/Al_2O_3	Fluidized bed	~600	~45	~93	Continuous regeneration	Low energy & CO_2; capital cost savings

(>18 wt% Cr). The process consists of four stages: reaction, product compression, separation, and refining. Countercurrent flow—hydrocarbons upward, air downward—improves yield and reduces raw material use. Typical operation is 650 °C, ~0.5 bar, achieving propylene selectivity >87%.[80] The heat-generating material (HGM) concept, co-loaded with catalyst, supplies reaction heat through cyclic redox, reducing external firing needs and cutting CO_2 emissions. First applied at commercial scale in 2012.[81]

4.3. FBD-4 process

The Snamprogetti FBD technology uses CrO_x/Al_2O_3 with metallic promoters. Propane conversion reaches ~45%, propylene selectivity ~80%. The circulating catalyst passes through a cyclone, with carbon-laden catalyst sent to a 700 °C regenerator. Heat from coke combustion drives the reaction section.[80]

4.4. STAR technology

The STAR process (Uhde/ThyssenKrupp, ex-Phillips) integrates ODH downstream of PDH to react hydrogen with oxygen to form water, shifting the PDH equilibrium and supplying exothermic heat to the endothermic step. Catalyst: Pt–Sn on Zn–Ca aluminate, high thermal stability in steam. Achieves high selectivity.[80]

4.5. PDH process

Linde's PDH process uses multi-tubular fixed-bed reactors with Pt–Sn catalysts, operating at 550–650 °C with periodic air regeneration. Selectivity can exceed 90%, catalyst life >2 years. Isothermal reactor control minimizes coke, reducing regeneration frequency.[80]

4.6. ADHO technology

Developed by China University of Petroleum (2016), implemented at Shandong Hengyuan Petrochemical. Catalyst: non-noble metal oxide, circulating fluidized bed, no pretreatment of feed (no desulfurization/arsenic removal). Handles propane, butane, or mixtures. Conversion and selectivity match FBD-4.[80,82]

4.7. K-PROt technology

KBR's K-PROt (2018) uses a non-precious, non-chromium dehydrogenation catalyst in a system adapted from KBR's catalytic olefins (K-COT™) process. Employs Orthoflow FCC-type continuous regeneration. Can operate standalone or integrated with steam cracking/FCC.[80]

4.8. FCDh process

Dow Chemical's FCDh (2016) applies FCC principles to fluidized catalytic dehydrogenation of propane, using K-promoted Pt–Ga/Al_2O_3. Achieves ~45% conversion, ~93% selectivity, with capital costs ~20% lower than other PDH routes.[80]

A summary of major PDH technologies is presented in Table 1.

5. The process of chemical looping ODHP

The anaerobic dehydrogenation technique presents certain limitations, including the inability to recycle the catalyst and restrictions imposed by thermodynamic equilibrium, which leads to diminished conversion efficiencies. Conversely, the aerobic dehydrogenation approach faces challenges, including the struggle to manage the extent of the reaction, particularly when employing CO_2 as the oxidizing agent, which results in inconsistent reaction outcomes. Chemical looping technology employs a regenerable oxygen carrier that gradually emits lattice oxygen to regulate the reaction's intensity, enhancing the thermodynamic irreversibility associated with conventional dehydrogenation processes. Chemical looping ODHP addresses the drawbacks associated with both oxidative and anaerobic dehydrogenation techniques, offering a promising approach to enhance the transformation of low-carbon alkanes and the selectivity for low-carbon olefins.[83–85]

Chemical looping ODHP consists of oxidation and reduction processes that depend on the type of reaction involving the oxygen carrier within two distinct reactors. The dehydrogenation reactor is where propane transforms with the assistance of an oxygen carrier material. This carrier material, after facilitating the dehydrogenation process, is then rejuvenated in a separate oxidation reactor using air. This re-oxygenation step not only replenishes the carrier but also generates heat. During this process, the byproducts of dehydrogenation, including low-carbon alkanes and hydrogen gas (H_2), interact with the lattice oxygen of the metal oxide carrier. This interaction leads to the formation of water, which is then removed through condensation. The removal of water effectively shifts the reaction equilibrium toward the desired direction, enhancing the conversion efficiency of the low-carbon alkanes. Under certain conditions, the lattice oxygen within the oxygen carrier can be gradually liberated, influencing the direction of the reaction and thereby improving the selectivity for propylene. After the oxygen carrier material is depleted of its active oxygen species within the dehydrogenation reactor, it is transported to a separate air reactor. Here, it encounters an abundance of oxygen from the air, initiating a process of re-oxidation. This re-oxidation step effectively replenishes the oxygen carrier, marking the completion of the regeneration cycle.[86] A flowchart showing this process is in Fig. 4.

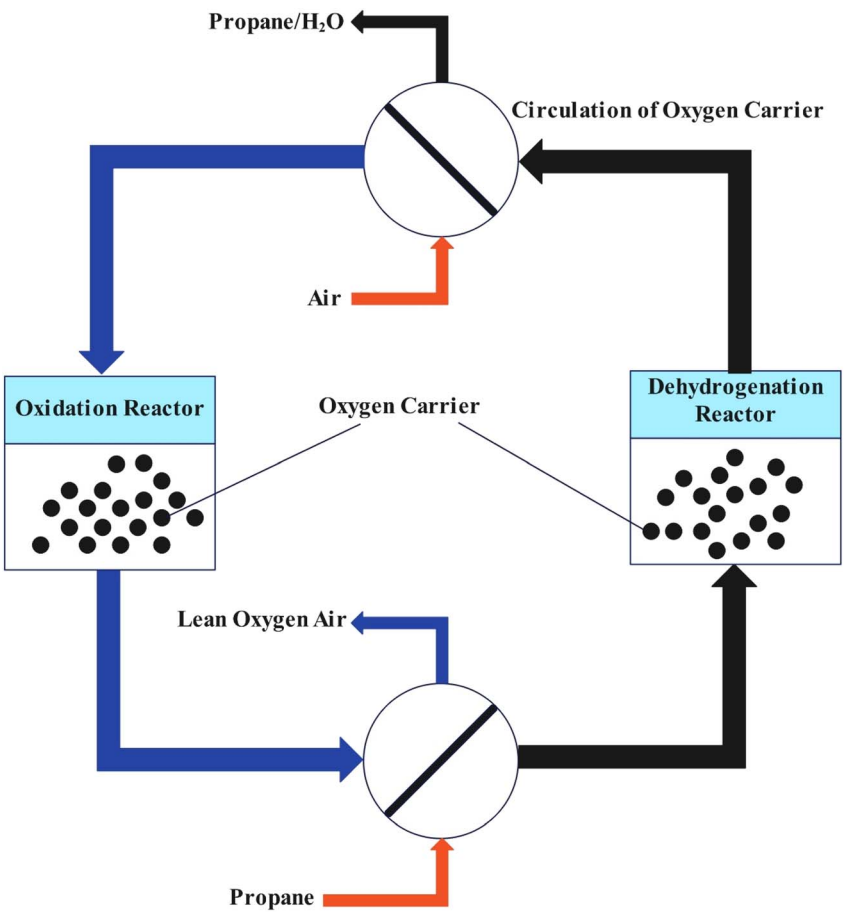

Fig. 4 Schematic of chemical looping ODHP, showing propane feed into the reduction reactor, propylene and by-products exiting to separation, oxygen-depleted carrier transfer to the oxidation reactor, re-oxidation with air, and return of the regenerated carrier. Heat exchange between reactors supports endothermic dehydrogenation.

Table 2 Comparison of oxygen carrier types in chemical looping ODHP[28,35,87–91]

Carrier type	Reaction temp. (°C)	Catalyst composition	Conversion (%)	Selectivity to propylene (%)	Cycle stability	Key advantages	Main limitations	Ref.
Monometallic	~615 optimal	VO_x/γ-Al_2O_3 (5–10 wt% V)	~11.7	~85.9	~10 cycles	Simple composition; high initial selectivity	Fast O release → overoxidation; limited life	87
Monometallic	540–650	Ga_2O_3, MoO_3, V_2O_5 carriers	Variable	Lower than V-based	10–15 cycles	High activity at lower temp (Ga)	Lower selectivity; faster deactivation	88
Bimetallic	550–600	VO_x/SiO_2 (alkoxy exchange)	~10–12	Higher than VO_x/SiO_2 physical mix	20+ cycles	Better dispersion of VO_x; improved selectivity	Still prone to sintering	35,89
Polymetallic	700 (ethane ODH)	$La_xSr_{2-x}FeO_{4-\delta}$	—	—	30 cycles	High oxygen capacity; stable cycling	Limited propane-specific data	28

5.1. Monometallic active oxygen carriers

A research team led by Al-Ghamdi *et al.* examined catalysts featuring different amounts of vanadium (5%, 7%, and 10% by weight), which were incorporated into γ-alumina, to study their performance in chemical looping ODHP processes. They attained a peak selectivity for propylene of 85.9% while achieving a conversion rate of 11.7% for propylene. Nonetheless, the VO_x/γ-Al_2O_3 catalysts exhibited a restricted cycle count, reaching a peak of 10 cycles during the entire reaction process. It was probably a result of the buildup of V_2O_5 crystalline formations on the catalyst's surface as the cycles progressed, leading to a reduction in propylene production. In single-metal oxygen transporters, the release of lattice oxygen occurs swiftly, leading to extensive oxidation of propane during the process of chemical looping ODHP. Extra CO_2 is frequently necessary to supply an oxygen source for the reaction environment. Applying suitable metal oxides to catalysts can help manage the pace at which lattice oxygen is released, as well as oversee the movement or generation of this released lattice oxygen from the catalyst surface. This approach may lower the selectivity for CO_x and prolong the durability of the catalyst.[87] Wu *et al.* evaluated the performance of oxygen carriers based on Ga, Mo, and V for the dehydrogenation of propane at temperatures of 540 °C, 615 °C, and 650 °C, respectively. The findings indicated that the oxygen carrier based on vanadium exhibited the highest level of catalytic efficiency. Additionally, the ideal temperature for the dehydrogenation of propane was determined to be 615 °C.[88]

5.2. Bimetallic or polymetallic composite oxygen carriers

Fukudome and colleagues successfully obtained elevated levels of isolated VO_x species by integrating them into the SiO_2 structure through an alkoxy exchange process involving polyethylene glycols and metal alcohol oxygen compounds. It was noted that VO_x incorporated into SiO_2 showed more significant selectivity for propylene than VO_x was simply added to SiO_2.[35,89] Gao and colleagues employed polymetallic composite oxygen carriers (La_x-$Sr_{2-x}FeO_{4-\delta}$) to convert ethane into ethylene, achieving an impressive yield of 51.6%, while the oxygen carriers underwent as many as 30 cycles. Consequently, it is essential to create oxygen carriers capable of enduring multiple cycles in the future.[28] Suitable bimetallic or even polymetallic oxides can gradually release lattice oxygen, which proves to be more efficient in regulating the propane dehydrogenation rate for propylene synthesis compared to gaseous oxidants and anaerobic dehydrogenation. Furthermore, metal oxides can impede the transformation of lattice oxygen (O^{2-}) into electrophilic oxygen (O^{2-}), leading to decreased oxide formation (*e.g.*, CO_x). It increases propylene selectivity and propane conversion rates.[20,90,91] The rapid response time of chemical looping ODHP, which varies from 20 seconds to 8 minutes, presents challenges in examining the reaction mechanism of propane dehydrogenation. To advance industrial growth, additional investigation is required to enhance oxygen carriers possessing a high capacity for oxygen loading and increased propane conversion while prioritizing propylene selectivity. Table 2 provides a comparison of oxygen carrier types in chemical looping ODHP.

6. Catalysts for ODHP based on vanadium

The development of catalysts for oxidative dehydrogenation of propane (ODHP) has largely focused on metal oxides, either used individually or in combination with promoters such as alkali halides and metals, supported on a variety of materials. Initially, unsupported catalysts were common, but supported vanadium catalysts have proven more advantageous due to better control over metal loading and dispersion, as well as the ability to fine-tune physicochemical properties. For example, TiO_2-supported catalysts containing $VOPO_4$ demonstrate higher ethylene selectivity than unsupported $(VO)_2P_2O_7$ or VO_x catalysts. Promoter incorporation has also been shown to enhance performance by separating reactive surface species and creating additional metal oxide phases on the support.[92,93]

Research into ODHP catalysts often distinguishes between high-temperature and low-temperature operation. High-temperature catalysts (>600 °C) are typically alkali or alkaline-earth oxides supported on rare-earth or transition-metal oxides, whereas low-temperature catalysts rely on reducible transition-metal oxides. While non-reducible alkaline and alkaline-earth oxides require high temperatures to achieve activity, this can lead to lower olefin selectivity. In contrast, reducible metal oxides can activate paraffins at lower temperatures, but often at the expense of selectivity due to overoxidation to CO_x. Vanadium oxides remain one of the most widely studied systems for ODHP because of their favorable crystal and electronic structure, as well as the multiple accessible oxidation states (V^{4+}/V^{5+}) that enable redox cycling.[34,36,94]

VO_x exhibits appropriate atomic arrangement and electronic configuration. Additionally, the presence of V^{4+} and V^{5+} valence levels enhances the significance of vanadium in numerous catalytic processes.[95] In addition, there has been considerable interest in backed vanadium oxides for their superior capabilities, improved heat resistance, and extensive specialized surface regions.

The stoichiometric formula for transforming propane through ODH into propylene using catalysts that contain vanadium is outlined as follows:

$$C_3H_8 + MO_x \rightarrow C_3H_8 + H_2O + MO_{x-1} \quad (5)$$

This diminished form of vanadium is restored through the use of molecular oxygen per the described chemical equation:

$$MO_{x-1} + \frac{1}{2}O_2 \rightarrow MO_x \quad (6)$$

The ODHP is typically governed by three primary factors when it comes to the redox activity of vanadium catalysts that are supported - namely, the surface structure of VO_x, the redox characteristics of the VO_x species, and the acid–base properties of both the metal and support. The support type and the amount of vanadium loaded are critical variables that impact these three properties.

6.1. VO_x surface coverage

The scientific publications have detailed the molecular configurations of vanadium species on metal oxide surfaces.[52,53] The research indicates that there are four possible types of VO_x surface species on the catalyst surface depending on the vanadium loading on the support: (a) isolated VO_4 units (monovanadates), (b) polymeric VO_4 structures (polyvanadates), (c) a mixture of isolated and polymeric VO_4, or (d) crystalline V_2O_5. Several research papers[96,97] have shown that low vanadium loading yields highly dispersed isolated VO_4 units, whereas increasing the loading leads to polymeric VO_4 due to higher surface coverage. Once the surface is saturated with a monolayer of VO_x, further increase in vanadium results in the formation of crystalline V_2O_5 particles. It is widely accepted that isolated tetrahedral VO_4 units (dominant at low loadings) favor higher selectivity in ODHP, while polymeric VO_4 structures provide higher activity.[96,97]

6.2. Effect of support (acid/base properties)

Metal oxides consist of metal cations and oxygen anions, but their catalytic function arises not only from redox cycling of the cations but also from dynamic participation of oxygen anions and vacancies that compensate framework charge. In vanadium oxides, for example, changes in V oxidation state (V^{5+}/V^{4+}) are balanced by the creation or annihilation of oxygen vacancies, which directly influence oxygen mobility and the nature of active oxygen species. Thus, the interplay between cations, anions, and lattice defects governs both redox capacity and catalytic selectivity. These materials have both acidic and basic properties, serving as Lewis acids and bases. Consequently, their acid–base characteristics can lead to various outcomes like dispersing active species, activating reactant molecules, shaping the structure of active components, influencing the rates of competing transformation routes, and affecting the desorption and adsorption rates of products and reactants.

In addition, the assistance provided by acid–base entities can impact both the reactivity of vanadium-based catalysts and the selectivity towards olefins.[98,99] For example, the bond between the acidic V_2O_5 molecules and an alkaline base like MgO, Sm_2O_3, or La_2O_3 could be robust. It could result in the creation of widely scattered VO_x particles, leading to elevated alkene selectivity. Conversely, the bond strength between the acidic V_2O_5 and an acidic substrate (for example, Al_2O_3, SiO_2) could be limited. It could result in a higher aggregation of vanadium species, promoting the emergence of a less potent crystalline phase of V_2O_5.[85,100]

Furthermore, acidic catalysts promote the adsorption of primary reactants and the desorption of acidic products. Consequently, this shields the chemical components from additional oxidation into carbon oxides. For example, more significant preferences for ethylene have been achieved with acid-based catalysts such as the catalysts comprised of VO_x/γ-Al_2O_3. The reason for these results was explained as the reduced interaction between the catalyst and the ethylene product due to increased support acidity.[101] Moreover, it is critical to maintain optimal levels of catalyst acidity and specific acid sites for

efficient olefin desorption and to prevent complete alkane oxidation to CO_x. It ensures that the catalyst activity and selectivity toward olefins are not compromised.[98]

6.3. Active lattice oxygen species

Beyond the configuration of the ODHP catalyst, a critical factor influencing the effectiveness and specificity of vanadium oxide catalysts on alumina support is the affinity of the surface lattice oxygen in the VO_x surface species. In comprehensive structural investigations of vanadium oxide catalysts on supports, researchers identified three distinct categories of lattice oxygen connections: (a) terminal V=O bonds, (b) V–O-support bonds, and (c) bridging V–O–V bonds. The binding strength varies for each category of lattice oxygen. The research focused on identifying the specific kind of connection between lattice oxygen atoms that plays a role in the oxidation activity observed in different catalytic oxidation processes.[83,102] In this catalytic oxidation reaction, it was found that the oxygen participating is the one present in the V–O-support bond, not in the terminal V–O–V or the V=O bonds.[102,103]

6.4. Exploring the redox characteristics of supported VO_x catalysts

One of the essential factors impacting the effectiveness of vanadium oxides in partial oxidation reactions is their ability to undergo reduction, which is especially important in alkane ODHP reactions. The connection between the surface structure and catalyst reducibility of VO_x on a specific metal oxide support is well established. With higher surface coverage of VO_x, the reducibility of the surface VO_x species tends to increase. Hence, the varying reducibility trend of the various vanadia species can be outlined as follows: polymeric surface VO_x surpasses isolated surface VO_x and crystalline V_2O_5 nanoparticles in reducibility.[104,105] In addition, the reducibility of vanadium oxide catalysts is influenced by the type of support utilized.

The acid–base nature of the catalyst support also influences its redox characteristics. An observation reveals a decline in the reducibility of vanadium species with the employment of increasingly alkaline support oxide materials.[106] Furthermore, the reaction for ODHP operating at temperatures between 450 and 550 °C revealed the following results: (a) the catalyst consisting of V_2O_5 supported on TiO_2, possessing lower basicity and being more comfortable to reduce, demonstrated the highest activity, (b) the catalyst comprising V_2O_5 supported on Al_2O_3, being more acidic and resistant to reduction, exhibited the highest selectivity towards propylene generation. The differences in the reducibility of vanadia oxide on various metal oxide supports might be linked to the varying reducibilities of the distinct V–O-support bonds present on different types of supports.[98,106]

As a result, it can be inferred that the performance and specificity of the vanadium oxide catalysts that are supported are greatly influenced by the characteristics of the supporting oxide material, the bonding of the surface VO_x components to the oxide support, and the quantity of vanadium applied. The sites responsible for redox facilitate the transfer of lattice oxygen to adsorbed propane for the production of propylene. The acid sites, on the other hand, promote the condensation of the intermediate substances. Hence, it is crucial to examine how the combined impacts of a catalyst's redox and acidic characteristics, along with their reliance on the catalyst's makeup and reaction circumstances, can be leveraged to improve the effectiveness of this procedure.

6.5. ODHP catalysts

To evaluate how these principles translate into practical catalyst design, a comparative survey of vanadium-based catalysts from recent studies is presented in Table 1. This table organizes catalysts by support type and lists their synthesis methods, key structural or mechanistic findings, and performance metrics. By grouping the data in this way, clear trends emerge—for example, the superior selectivity of silica-incorporated isolated VO_4 species, the thermal stability advantages of ceria-modified titania nanotubes, and the confinement effects observed in MOF-supported vanadium. Such comparisons provide valuable guidance for future ODHP catalyst development, especially for industrial applications where both selectivity and durability are critical.

Recent investigations have reinforced the central role of vanadium in dictating the selectivity, activity, and stability of ODHP catalysts. Vanadium's ability to cycle between V^{5+}/V^{4+} oxidation states enable the Mars–van Krevelen redox mechanism, where lattice oxygen species (O^{2-}, O^-) participate in selective C–H bond activation while minimizing over-oxidation when properly tuned. Al Abdulghani *et al.* demonstrated that incorporating Ta^{5+} into VO_x/SiO_2 accelerates the re-oxidation of reduced vanadium centers, maintaining them in their most selective state and suppressing the formation of electrophilic oxygen species that promote CO_x formation. *Operando* studies revealed that vanadium sites can generate isopropanol intermediates, with over-oxidation routes involving propylene epoxidation—underscoring the need to manage lattice oxygen reactivity through promoter selection.[107]

Passamonti *et al.* systematically varied vanadium loading on γ-Al_2O_3, showing that ~7–8 wt% V maximizes propylene yield by balancing VO_4 dispersion and polymerization. Low V loading favors isolated tetrahedral VO_4 units with high selectivity but lower activity, while high loading promotes polyvanadate networks and V_2O_5 crystallites that enhance activity but increase deep oxidation. This confirms that vanadium's surface speciation—dictated by loading and support interaction—is a primary control lever in ODHP design.[108]

Mandal *et al.*, using advanced quantum chemistry, found that the initial C–H activation barrier over VO_x sites is sensitive to electronic correlation and active site geometry. Cooperative vanadium site arrangements were predicted to reduce activation energy compared to isolated sites, suggesting that engineering adjacent VO_x moieties could amplify turnover rates without compromising selectivity.[109] Mesa *et al.* extended the strategy to CO_2-assisted ODHP over VO_x/CHA zeolites, where vanadium's redox flexibility synergizes with CO_2 to shift equilibria, suppress coke, and stabilize active oxygen species. Their

Table 3 Performance of vanadium-based catalysts in ODHP

Support type	Catalyst	Synthesis method	Reaction conditions	Key findings	Performance	Ref.
Silica-based	VO_x in SiO_2 framework	Alkoxy exchange with PEG & metal alkoxide	Fixed-bed, 450 °C; feed C_3H_8/Ar = 5/20 mL min^{-1} (also tested neat propane = 5 mL min^{-1}); catalyst 200 mg; pretreat in O_2/Ar = 5/20 mL min^{-1}	Isolated VO_4^{3-} species enhanced propylene selectivity	88.3% selectivity, 26.5% conversion, stable over 10 cycles at 450 °C	89
	V-KIT-6 (5 wt% V)	Direct hydrothermal, pH 5	600 °C operation noted; tests at 525 °C with varied total flow to adjust conversion; constant space velocity used	Maintained 3D mesoporous structure, improved VO_x dispersion	C_2H_4 + propylene selectivity 70.2%, STY 3.9 kg kg_{cat}^{-1} h^{-1}	111
	Monomeric/dimeric VO_x on SiO_2	DFT modeling	—	Dimer species lower activation barrier for C–H activation	Rate constants 14% higher for dimer + monomer mix at 750 K	112
	Ta-promoted V/SiO_2	Impregnation	ODH reaction temperatures (400−500 °C); WHSV 28−170 (g propane g_{cat}^{-1} h^{-1}); 30% propane/15% O_2/55% N_2	Ta promotion improved ODHP selectivity *vs.* B-based catalysts	Higher conversion and selectivity than B-based systems (exact % not specified)	107
	VO_x/SBA-15	Impregnation	—	Mesoporous SBA-15 enhanced dispersion and stability	—	109
Alumina-based	VO_x/γ-Al_2O_3 (7.5 wt% V)	Wet impregnation	CREC fluidized-bed riser, O_2-free ODHP; 475–550 °C; consecutive propane injections (*e.g.*, 10 mL per shot)	Monomeric at low loading, polymeric at higher loading	11.7–15.1% conversion, 67.6–85.9% selectivity (475–550 °C)	10
	VO_x/γ-Al_2O_3–CaO (1 : 1)	Wet impregnation	*T*: 640 °C; Cat.: 0.5 g; propane injected: 1.2 mL	CaO improved basicity and activity	25.5% conversion, 94.2% selectivity at 640 °C	113
	V(x)/Al_2O_3 (1–11 wt% V)	Wet impregnation	Fixed-bed; m_{cat} = 100 mg; propane/O_2 = 2.5 (propane 15 cm^3 min^{-1}) with N_2 balance; 300–550 °C	Optimal propylene selectivity at 6 wt% V loading	Conversion varies; maximum at intermediate loading, selectivity peak at 6 wt% V	108
	VO_x/Carbon nanofibers (CNF)	Chemical vapor deposition + impregnation	ODHP at 600 °C, 0.9 bar g; feed CO_2/propane/N_2 = 2.5 : 2.5 : 5 N mL min^{-1}; GHSV = 3.0 × 10^3 h^{-1}; WHSV = 1.5 $g_{propane}$ g_{cat}^{-1} h^{-1}	CNF support provided high surface area and conductivity	27.1% conversion, 92.3% selectivity at 540 °C	110
	VO_x–Ga/γ-Al_2O_3	Incipient wetness impregnation	Fixed-bed, continuous flow; propane/O_2/Ar co-feed; 0.5 g_{cat}; 325–500 °C; varied GHSV	Highly dispersed, tetrahedral monomeric VO_x with Ga^{3+} Lewis sites; stable activity at low temperature	Reported stable ODHP at 400 °C	114

Table 3 (*Contd.*)

Support type	Catalyst	Synthesis method	Reaction conditions	Key findings	Performance	Ref.
Carbon-based	V_2O_5/graphene	Hydrothermal	Fixed-bed; 450 °C; propane/air ratio = 0.6; total flow 90 mL min^{-1}	Optimal C : V ratio 1 : 1 improved performance	50.7% conversion, 53.6% selectivity at 450 °C	115
	V_2O_5/SWCNT, MWCNT	Reflux/hydrothermal	Fixed-bed; 450 °C; propane/air ratio = 0.6; total flow 90 mL min^{-1}	CNT supports improved dispersion	Moderate activity/selectivity depending on CNT type	115
Mixed-oxide	VO_x/γ-Al_2O_3–ZrO_2 (1 : 1)	Wet impregnation	Tests at 600–650 °C	Best balance of activity/selectivity at 7.5 wt% V	25% conversion, 94% selectivity, CO_x 2.1% at 550 °C	38,116
	VO_x/θ-Al_2O_3–CaO	Deposition	*T*: 500 °C; 3.6 wt% V_2O_5/ZrO_2; P/V = 1 catalyst	Reduced CO_x formation	Lower CO_x *vs.* base θ-Al_2O_3	117
	VO_x/θ-Al_2O_3–BaO	Deposition	T: 500 °C; 3.6 wt% V_2O_5/ZrO_2; P/V = 1 catalyst	Increased olefin yield	Olefin yield 49%	117
	V_2O_5–phosphate/ZrO_2	Co-deposition	Fixed-bed; 723–823 K; feed propane 6 vol%/O_2 3 vol%/N_2 91 vol%; total flow 60 mL min^{-1}; 1 atm	Phosphate stabilized tetragonal ZrO_2, improved acidity	Conversion ↑ from 12% to 20%, selectivity ↑ from 54% to 64%	118
	V_2O_5/TiO_2	Impregnation	ODHP runs 450–550 °C	Lower basicity, higher reducibility → high activity	High propylene yield at 450–550 °C	106
	VO_x/CeO_2	Impregnation	One sample: V loading = 0.57 V nm^{-2}, *T* = 550 °C	CO_2-assisted ODHP: nuclearity-dependent behavior; ceria oxygen vacancies play roles in side reactions; monomeric VO_x helps reduce over-oxidation	Partial selectivity/conversion values for several loadings (some high nuclearity samples have more CO_x)	119
MOF-based	V_2O_5/UiO-66	Ultrasonic-assisted impregnation	Tests at 350 °C	Confinement effect improved ODHP performance	17.1% conversion, 49.7% selectivity, productivity 4.4 g g_{cat}^{-1} h^{-1} at 350 °C	120
Other supports	VO_x/h-BN	Dispersion method	Fixed-bed; typical ODHP feeds such as propane/O_2/N_2 = 1 : 1 : 38 and 1:2:37; GHSV ≈ 18 000 mL g_{cat}^{-1} h^{-1}	BO_x active sites and VO_x redox synergy enhanced activity	Doubled C_2–C_3 olefin yield at 540–580 °C with 0.5% V	121
	Monomeric/dimeric VO_x on TiO_2	Grafting & dehydration	—	Coordination environment critical for activity	Up to 800× increase in C–H activation rate at 600 K	122
	VO_x/Ti_3AlC_2	Impregnation	*T* approx 550–600 °C; feed includes propane + O_2 (co-feed), but exact molar ratios/WHSV/GHSV are not fully reported in visible parts	Good propane ODH performance; shows better stability and high selectivity when VO_x is highly dispersed on MAX	Conversion & selectivity numbers not fully extracted in available view; best reported selectivity ≈ 85–90% under studied conditions	123
	VO_x–CeO_2/γ-Al_2O_3	Co-precipitation/impregnation	Fixed bed mode, propane feed with lattice oxygen (chemical looping), no molecular O_2 in reaction step	Ce addition moderates lattice oxygen release, reduces over-oxidation, increases propylene selectivity and stability over cycles	At 550 °C, 10V–3Ce/Al: ∼81.9% selectivity to propylene, CO_x ∼7.3%, stable over 15 cycles *vs.* ∼62.8% sel., CO_x ∼25.6% for 10V/Al (no Ce)	124

results indicate that pairing vanadium's inherent redox capability with tailored reaction environments can both improve performance and deliver CO_2 utilization benefits.[110]

Key vanadium-centered strategies emerge: (i) control VO_x loading to tune the monomer/polymer/crystalline balance; (ii) use promoters that enhance vanadium's redox cycling while limiting over-oxidation; (iii) select supports that optimize VO_x dispersion and stabilize tetrahedral species (*e.g.*, SiO_2, TiO_2, CHA zeolite, ZrO_2 composites); (iv) design catalysts with cooperative vanadium site architectures to lower C–H activation barriers; and (v) integrate vanadium catalysts with reaction modifiers (*e.g.*, CO_2 co-feeding) to exploit redox flexibility and improve long-term stability.

Table 3 summarizes the performance of various vanadium-based catalysts in the ODHP process.

Vanadium-based catalysts play a central role in ODHP because of their ability to cycle between V^{5+} and V^{4+} oxidation states, enabling participation in the Mars–van Krevelen mechanism. In this process, lattice oxygen species from VO_x oxidize propane to propylene, and the reduced vanadium is re-oxidized by molecular oxygen or other oxidants. The nature of the support, the dispersion of VO_x species, the oxygen mobility, and the acid–base properties of the catalytic surface all determine the selectivity, activity, and stability of the system. The table shows that silica-based supports, being relatively inert and acidic, tend to stabilize isolated tetrahedral VO_4 units, which favor high propylene selectivity but moderate activity. Mesoporous silica structures such as KIT-6 or SBA-15 improve VO_x dispersion and accessibility, while certain promoters, such as tantalum, enhance the redox cycling of vanadium and suppress the formation of over-oxidizing electrophilic oxygen. In contrast, alumina-based supports, with their stronger V–O-support interactions, allow higher vanadium loadings but also present a risk of deep oxidation due to their acidity. Modifying alumina with basic oxides such as CaO can weaken olefin adsorption, thereby improving selectivity. Optimal vanadium loadings prevent excessive polymerization of VO_x species, which otherwise leads to lower selectivity. Carbon-based supports like graphene, carbon nanotubes, and carbon nanofibers provide high surface area, good dispersion, and in some cases enhanced electronic conductivity, which can accelerate redox turnover and boost both activity and selectivity.

Mixed-oxide supports, such as ZrO_2- or TiO_2-modified systems, fine-tune acidity, basicity, and oxygen mobility, enabling high propylene selectivity and thermal stability. The addition of modifiers like phosphate or alkaline earth metals can further adjust the balance of acid–base properties and stabilize favorable crystal phases. Metal–organic frameworks, such as UiO-66, offer confinement effects that prevent VO_x sintering and preserve dispersion, supporting stable operation and consistent productivity. Other unique supports, including hexagonal boron nitride and TiO_2, influence the coordination environment of VO_x species in ways that significantly affect C–H activation rates.

Across all support types, the function of vanadium in ODHP is governed by several interconnected factors. The redox cycle between V^{5+} and V^{4+} ensures the supply of lattice oxygen, while the nature of the support controls the type of oxygen species generated, balancing nucleophilic oxygen for selectivity against electrophilic oxygen that promotes over-oxidation. Dispersion and polymerization levels of VO_x determine the trade-off between activity and selectivity, with monomeric VO_4 species favoring propylene production and polymeric species increasing total activity but also the risk of side reactions. Support interactions modify acidity and basicity, influencing olefin desorption and preventing complete oxidation to CO_x, while electronic effects from promoters or conductive supports adjust the electron density at vanadium sites to optimize catalytic performance. Together, these parameters define the efficiency, selectivity, and durability of vanadium-based ODHP catalysts.

7. Commercial strategies in PDH

The process of propane dehydrogenation for commercial purposes is conducted explicitly without the presence of an oxidizing agent. A variety of technologies are currently utilized, employing different catalysts derived from Cr or Pt. The utilization of alkali metal-enhanced Pt–Sn Al_2O_3 catalysts in a system consisting of four continuously moving bed reactors characterizes the OLEFLEX procedure developed by UOP. Throughout this procedure, the catalyst is consistently renewed within an isolated regeneration loop. The reactor units are arranged sequentially alongside gas flow pre-heaters, functioning at pressures ranging from 1 to 3 bar at temperatures around 650 °C. In the OLEFLEX procedure, the usual catalyst is comprised of rounded pellets made of γ-Al_2O_3 (with an approximate surface area of 100 square meters per gram) that include less than 1 w% of Pt, enhanced with Sn and alkali metals.[3]

The Dow FCDh technology makes use of a fluidized reactor system in conjunction with a fluidized regeneration reactor, allowing for uninterrupted operation and regeneration.[125] The catalyst consists of an Al_2O_3 support that is commercially obtained and treated with Pt and Ga. The catalyst has the potential to be entirely regained following the regeneration process, which requires subjecting it to a high-temperature oxidative treatment to eliminate any stored carbon elements, also known as coke. In contrast to the complex regeneration process of the OLEFLEX method involving H_2, O_2, and Cl_2, the Dow FCDh technology allows for a significantly streamlined regeneration procedure.[3]

The STAR process, known as Steam Active Reforming, is utilized by Phillips Petroleum and was created by Uhde. It utilizes a Pt catalyst that is promoted by Sn (0.2 to 0.6 wt%), distributed on a support composed of zinc-aluminate and bound by magnesium/calcium aluminate. The process operates at pressures ranging from 6 to 9 bar and temperatures between 550 and 590 °C.[126] Additionally, because it is not acidic, the catalyst does not encourage unwanted side reactions like isomerization, cracking, or coke formation. It includes Sn as a promoter to minimize coke formation and enhance selectivity. Progress in developing catalysts for the STAR procedure is ongoing, as shown by the collaboration between BASF and

Thyssenkrupp in 2020. Their joint effort focuses on cutting down on carbon dioxide emissions, minimizing raw material usage, and lowering operational expenses. It highlights the potential for enhancing established processes through advancements in catalyst design.[3]

The substance known as chromium oxide on aluminium oxide (CrO_x/Al_2O_3) is frequently used in industrial settings within the CATOFIN process. It consists of around 18–20% chromium oxide supported by 1–2% alkaline metal (either K or Na) promoted aluminium oxide.[126] The presence of alkali promoters significantly impacts the catalyst's performance by altering its surface acidity. Specifically, alkali promoters reduce the acidity of the alumina support, thereby minimizing unwanted side reactions and improving both the catalyst's activity and its ability to produce the desired products. Enhancements to both the catalyst composition and operating conditions have been implemented within the commercial CATOFIN process.[3]

Nevertheless, persisting issues remain concerning the durability, specificity, and effectiveness of the catalysts. To increase propylene production and lower emissions, the use of a heat-producing substance known as HGM has been implemented, with Clariant being a prominent developer of such technology. The precise makeup of the HGM catalyst likely incorporates copper oxide as its primary component, along with supplemental promoters such as manganese dioxide (MnO_2). These components are typically supported on a substrate of alpha-alumina (α-Al_2O_3). The reactor contains the catalyst, transforming it as the reaction progresses. This process produces heat, counterbalancing the heat consumed in the reaction. Ever since the introduction in 2015 at Ningbo Haiyue New Material Co. situated in Ningbo City, China, the identical HGM technology has been incorporated into more CATOFIN operations, and Ineos has recently granted Clariant a lengthy agreement to provide the HGM.[3]

K-PRO, created by KBR, is the most recent process that has been brought into the commercial market. The inaugural agreement was issued in January 2020, about one year subsequent to the technology's introduction, and subsequently, a licensing deal has been established with JS Energy Ltd. The importance of this procedure lies in the fact that the catalyst lacks valuable metals or chromium, while the specific component(s) remain undisclosed proprietary details. The reactor design utilizes KBR's FCC Orthoflow reactor, functioning as an ascending vertical reactor riser. It shares similarities with the Dow FCDh process in terms of being a fluidized bed configuration, although the regeneration segment differs.[3]

8. Conclusion and outlook

This comprehensive review has highlighted the significant role of vanadium-based catalysts in ODHP. It has explored the thermodynamic and environmental considerations of various dehydrogenation methods, highlighting the advantages of ODHP in terms of energy efficiency and reduced CO_2 emissions. The review has also identified the active site in ODHP, emphasizing the importance of vanadium dispersion and coordination geometry within the support material.

Across a wide range of support types, from silica- and alumina-based systems to mixed oxides, carbon materials, and MOFs, the function of vanadium in ODHP is closely tied to its redox cycling between V^{5+} and V^{4+} states, which enables lattice oxygen participation *via* the Mars–van Krevelen mechanism. The results demonstrate that isolated VO_4 species on inert supports such as mesoporous silica favor high propylene selectivity (up to 88.3%) with good stability, while basicity modification of alumina (*e.g.*, with CaO) can suppress deep oxidation and raise selectivity above 94%. Mixed-oxide supports like γ-Al_2O_3–ZrO_3 or phosphate-modified ZrO_2 optimize acidity and oxygen mobility to balance activity and selectivity, achieving propylene yields above 90% with minimal CO_x formation. Carbon nanofiber and graphene supports provide high dispersion and conductivity, boosting selectivity and conversion simultaneously, and MOF-based systems such as V_2O_5/UiO-66 leverage confinement effects to maintain dispersion and stability. The four recent studies further reveal how promoters like Ta, advanced mesoporous supports, and optimal vanadium loadings fine-tune the balance between monomeric and polymeric VO_x species, thereby controlling the trade-off between activity and selectivity.

The review showcased various strategies for improving the performance of vanadium catalysts. The selection of support materials with specific properties, such as enhanced thermal stability, larger surface area, and suitable pore structure, has proven critical for achieving superior activity and selectivity. Furthermore, the synthesis methods, particularly co-assembly and impregnation techniques, have been shown to impact the bonding between vanadium species and the support, ultimately influencing catalytic performance.

The review has also discussed the implementation of chemical looping ODHP, a promising technology for further enhancing the efficiency and sustainability of the process. This approach, coupled with the development of novel vanadium catalysts, presents significant potential for overcoming existing challenges, such as coke formation and catalyst deactivation.

Moving forward, continued research efforts should focus on the following key areas:

8.1. Developing novel support materials

The search for high-performance supports with optimized properties, including enhanced thermal stability, improved redox properties, and tailored pore structures, is critical. This includes exploring the potential of emerging materials like MOFs, zeolites, and carbon-based materials.

8.2. Tailoring vanadium species

Understanding the interplay between vanadium dispersion, coordination geometry, and catalytic performance requires further investigation. This includes exploring different vanadium precursors, optimization of synthesis methods, and fine-tuning the interaction between vanadium and the support.

8.3. Optimizing reactor design

Developing innovative reactor designs that minimize coke formation, enhance mass transfer, and improve heat management is crucial for achieving high propylene yields and long catalyst lifetimes.

8.4. Integration of chemical looping ODHP

Further research into chemical looping ODHP, including optimization of the redox cycle, development of robust oxygen carriers, and integration of this technology with existing industrial processes, is essential for achieving sustainable and cost-effective propylene production.

By addressing these research priorities, the field of vanadium catalysts for ODHP can further advance, paving the way for the development of efficient, selective, and sustainable propylene production processes.

Author contributions

Erfan Nouri: conceptualization, methodology, writing – original draft, and review, data collection, analysis of existing literature, and writing – sections on current technologies. Zeynab Dabirifar: data collection, analysis of literature, and visualization of results. Alireza Kardan: writing – sections on challenges and future directions, and review of the manuscript, data analysis, visualization of results, and contributions to discussion sections. Mojtaba Saei Moghaddam: supervision, project management, and final editing of the manuscript.

Conflicts of interest

Authors have no conflict of interest to declare.

Data availability

This review article does not contain any original datasets. The information presented is based on previously published studies and publicly available data. All relevant data and materials cited in this review are referenced appropriately throughout the text.

References

1 V. Manokaran, P. Saiprasad and S. Srinath, *Procedia Eng.*, 2015, **127**, 1338–1345.
2 X. Jiang, L. Sharma, V. Fung, S. J. Park, C. W. Jones, B. G. Sumpter, J. Baltrusaitis and Z. Wu, *ACS Catal.*, 2021, **11**, 2182–2234.
3 A. M. Gaffney and O. M. Mason, *Catal. Today*, 2017, **285**, 159–165.
4 Z. Zhai, X. Wang, R. Licht and A. T. Bell, *J. Catal.*, 2015, **325**, 87–100.
5 S. Rostom and H. de Lasa, *Catalysts*, 2020, **10**, 418.
6 A. Darvishi, R. Davand, F. Khorasheh and M. Fattahi, *Chin. J. Chem. Eng.*, 2016, **24**, 612–622.
7 A. A. Ayandiran, I. A. Bakare, H. Binous, S. Al-Ghamdi, S. A. Razzak and M. M. Hossain, *Catal. Sci. Technol.*, 2016, **6**(13), 5154–5167.
8 A. H. Elbadawi, M. S. Osman, S. A. Razzak and M. M. Hossain, *J. Taiwan Inst. Chem. Eng.*, 2016, **61**, 106–116.
9 Y. Chen, B. Yan and Y. Cheng, *Catalysts*, 2023, **13**, 204.
10 S. A. Al-Ghamdi and H. I. de Lasa, *Fuel*, 2014, **128**, 120–140.
11 R. Koirala, R. Buechel, S. E. Pratsinis and A. Baiker, *Appl. Catal., A*, 2016, **527**, 96–108.
12 B. Barghi, M. Fattahi and F. Khorasheh, *Pet. Sci. Technol.*, 2014, **32**, 1139–1149.
13 F. Cavani and F. Trifirò, *Catal. Today*, 1995, **24**, 307–313.
14 S. N. Khadzhiev, N. Y. Usachev, I. M. Gerzeliev, E. P. Belanova, V. P. Kalinin, V. V. Kharlamov, A. V. Kazakov, S. A. Kanaev, T. S. Starostina and A. Y. Popov, *Pet. Chem.*, 2015, **55**, 651–654.
15 A. Z. Varzaneh, M. S. Moghaddam and J. T. Darian, *Pet. Chem.*, 2018, **58**, 13–21.
16 M. S. Moghaddam and J. Towfighi, *Pet. Chem.*, 2018, **58**, 659–665.
17 M. Saei Moghaddam and J. Towfighi, *J. Chem. Pet. Eng.*, 2017, **51**, 113–121.
18 A. Al-Mamoori, S. Lawson, A. A. Rownaghi and F. Rezaei, *Appl. Catal., B*, 2020, **278**, 119329.
19 B. R. Jermy, B. Ajayi, B. Abussaud, S. Asaoka and S. Al-Khattaf, *J. Mol. Catal. A: Chem.*, 2015, **400**, 121–131.
20 M. Fattahi, M. Kazemeini, F. Khorasheh and A. Rashidi, *Chem. Eng. J.*, 2014, **250**, 14–24.
21 G. Tanimu, A. Aitani, S. Asaoka and H. Alasiri, *Mol. Catal.*, 2020, **488**, 110893.
22 D. Mukherjee, S.-E. Park and B. M. Reddy, *J. CO2 Util.*, 2016, **16**, 301–312.
23 C. Carrero, M. Kauer, A. Dinse, T. Wolfram, N. Hamilton, A. Trunschke, R. Schlögl and R. Schomäcker, *Catal. Sci. Technol.*, 2014, **4**, 786–794.
24 H. J. Dar, S. U. Nanot, K. J. Jens, H. A. Jakobsen, E. Tangstad and D. Chen, *Ind. Eng. Chem. Res.*, 2012, **51**, 10571–10585.
25 I. I. Mishanin, A. N. Kalenchuk, K. I. Maslakov, V. V. Lunin, A. E. Koklin, E. D. Finashina and V. I. Bogdan, *Russ. J. Phys. Chem. A*, 2016, **90**, 1132–1136.
26 S. Ahmed, F. Rahman, A. M. J. Al-Amer, E. M. Al-Mutairi, U. Baduruthamal and K. Alam, *React. Kinet., Mech. Catal.*, 2012, **105**, 483–493.
27 I. Gerzeliev, A. Y. Popov and V. Ostroumova, *Pet. Chem.*, 2016, **56**, 724–729.
28 Y. Gao, L. M. Neal and F. Li, *ACS Catal.*, 2016, **6**, 7293–7302.
29 J. C. Védrine, *Catalysts*, 2016, **6**(2), 22.
30 P. Wang, X. Zhang, R. Shi, J. Zhao, G. I. Waterhouse, J. Tang and T. Zhang, *Nat. Commun.*, 2024, **15**, 789.
31 M. A. Artsiusheuski, R. Verel, J. A. van Bokhoven and V. L. Sushkevich, *Angew. Chem., Int. Ed.*, 2023, **62**, e202309180.
32 Z. Geng, Y. Zhang, H. Deng, S. Wang and H. Dong, *Chem. Eng. Res. Des.*, 2023, **195**, 235–246.
33 F. Xing and S. Furukawa, *Chem. – Eur. J.*, 2023, **29**, e202202173.

34 M. M. Hossain, *Ind. Eng. Chem. Res.*, 2017, **56**, 4309–4318.
35 K. Fukudome, N.-o. Ikenaga, T. Miyake and T. Suzuki, *Catal. Today*, 2013, **203**, 10–16.
36 S. Rostom and H. I. de Lasa, *Ind. Eng. Chem. Res.*, 2017, **56**, 13109–13124.
37 D. Luo, R. Luo, X. Wang, X. Chang, T. Yang, S. Chen, Z.-J. Zhao and J. Gong, *Chem. Sci.*, 2025, **16**, 4710–4717.
38 Y. Zaynali and S. M. Alavi-Amleshi, *Part. Sci. Technol.*, 2017, **35**, 667–673.
39 J. Rischard, C. Antinori, L. Maier and O. Deutschmann, *Appl. Catal., A*, 2016, **511**, 23–30.
40 K. Chen, A. Khodakov, J. Yang, A. T. Bell and E. Iglesia, *J. Catal.*, 1999, **186**, 325–333.
41 E. Gomez, S. Kattel, B. Yan, S. Yao, P. Liu and J. G. Chen, *Nat. Commun.*, 2018, **9**, 1398.
42 F. T. Zangeneh, A. Taeb, K. Gholivand and S. Sahebdelfar, *Chem. Eng. Commun.*, 2016, **203**, 557–565.
43 M. Aresta, A. Dibenedetto and E. Quaranta, *J. Catal.*, 2016, **343**, 2–45.
44 A. Abdulrasheed, A. A. Jalil, Y. Gambo, M. Ibrahim, H. U. Hambali and M. Y. S. Hamid, *Renewable Sustainable Energy Rev.*, 2019, **108**, 175–193.
45 C.-J. Pan, M.-C. Tsai, W.-N. Su, J. Rick, N. G. Akalework, A. K. Agegnehu, S.-Y. Cheng and B.-J. Hwang, *J. Taiwan Inst. Chem. Eng.*, 2017, **74**, 154–186.
46 Y. Wang, P. Han, X. Lv, L. Zhang and G. Zheng, *Joule*, 2018, **2**, 2551–2582.
47 H. Li, L. Li and Y. Li, *Nanotechnol. Rev.*, 2013, **2**, 515–528.
48 C. Wang, F. Feng, J. Du, T. Zheng, Z. Pan and Y. Zhao, *ChemCatChem*, 2019, **11**, 2054–2057.
49 J. C. Védrine, *Catalysts*, 2016, **6**, 22.
50 A. Alamdari, R. Karimzadeh and S. Abbasizadeh, *Rev. Chem. Eng.*, 2021, **37**, 481–532.
51 J. T. Grant, J. M. Venegas, W. P. McDermott and I. Hermans, *Chem. Rev.*, 2017, **118**, 2769–2815.
52 X. Gao, J.-M. Jehng and I. E. Wachs, *J. Catal.*, 2002, **209**, 43–50.
53 I. Rossetti, G. F. Mancini, P. Ghigna, M. Scavini, M. Piumetti, B. Bonelli, F. Cavani and A. Comite, *J. Phys. Chem. C*, 2012, **116**, 22386–22398.
54 L. Jalowiecki-Duhamel, A. Ponchel, C. Lamonier, A. D'Huysser and Y. Barbaux, *Langmuir*, 2001, **17**, 1511–1517.
55 R. You, X. Zhang, L. Luo, Y. Pan, H. Pan, J. Yang, L. Wu, X. Zheng, Y. Jin and W. Huang, *J. Catal.*, 2017, **348**, 189–199.
56 K. Niu, L. Chi, J. Rosen and J. Björk, *Phys. Chem. Chem. Phys.*, 2020, **22**, 18622–18630.
57 Z. Zhao, C. Chiu and J. Gong, *Science*, 2015, **6**, 4403–4425.
58 L. Ma, Y. Geng, X. Chen, N. Yan, J. Li and J. W. Schwank, *Chem. Eng. J.*, 2020, **402**, 125911.
59 E. V. Kondratenko and A. Brückner, *J. Catal.*, 2010, **274**, 111–116.
60 B. Qiu, F. Jiang, W.-D. Lu, B. Yan, W.-C. Li, Z.-C. Zhao and A.-H. Lu, *J. Catal.*, 2020, **385**, 176–182.
61 J. T. Grant, C. A. Carrero, F. Goeltl, J. Venegas, P. Mueller, S. P. Burt, S. Specht, W. McDermott, A. Chieregato and I. Hermans, *Science*, 2016, **354**, 1570–1573.
62 C. Si, Z. Lian, S. O. Olanrele, X. Sun and B. Li, *Appl. Surf. Sci.*, 2020, **519**, 146241.
63 W.-D. Lu, D. Wang, Z. Zhao, W. Song, W.-C. Li and A.-H. Lu, *ACS Catal.*, 2019, **9**, 8263–8270.
64 L. Shi, D. Wang, W. Song, D. Shao, W. P. Zhang and A. H. Lu, *ChemCatChem*, 2017, **9**, 1788–1793.
65 X. Sun, J. Wu, Q. Liu and F. Tian, *Appl. Surf. Sci.*, 2018, **455**, 864–875.
66 Z. Zhao, G. Ge, W. Li, X. Guo and G. Wang, *Chin. J. Catal.*, 2016, **37**, 644–670.
67 B. Li and D. Su, *Chem. – Eur. J.*, 2014, **20**, 7890–7894.
68 R. Huang, J. Xu, J. Wang, X. Sun, W. Qi, C. Liang and D. S. Su, *Carbon*, 2016, **96**, 631–640.
69 L. Liu, Q.-F. Deng, B. Agula, T.-Z. Ren, Y.-P. Liu, B. Zhaorigetu and Z.-Y. Yuan, *Catal. Today*, 2012, **186**, 35–41.
70 X. Sun, Y. Ding, B. Zhang, R. Huang and D. S. Su, *Chem. Commun.*, 2015, **51**, 9145–9148.
71 L. Cao, P. Dai, L. Zhu, L. Yan, R. Chen, D. Liu, X. Gu, L. Li, Q. Xue and X. Zhao, *Appl. Catal., B*, 2020, **262**, 118277.
72 R. Schlögl, *Top. Catal.*, 2011, **54**, 627–638.
73 J. C. Védrine and I. Fechete, *C. R. Chim.*, 2016, **19**, 1203–1225.
74 V. V. Kaichev, Y. A. Chesalov, A. A. Saraev and A. M. Tsapina, *J. Phys. Chem. C*, 2019, **123**, 19668–19680.
75 Y. Zhang, J. Tang, M. Li, Y. Shu, F. Wang, W. Cao and Z. Wu, *Mater. Sci. Eng., C*, 2018, **92**, 1–10.
76 T. Otroshchenko, O. Bulavchenko, H. V. Thanh, J. Rabeah, U. Bentrup, A. Matvienko, U. Rodemerck, B. Paul, R. Kraehnert, D. Linke and E. V. Kondratenko, *Appl. Catal., A*, 2019, **585**, 117189.
77 A. Perechodjuk, Y. Zhang, V. A. Kondratenko, U. Rodemerck, D. Linke, S. Bartling, C. R. Kreyenschulte, G. Jiang and E. V. Kondratenko, *Appl. Catal., A*, 2020, **602**, 117731.
78 J. F. S. de Oliveira, D. P. Volanti, J. M. C. Bueno and A. P. Ferreira, *Appl. Catal., A*, 2018, **558**, 55–66.
79 S. Luo, L. Zeng and L.-S. Fan, *Annu. Rev. Chem. Biomol. Eng.*, 2015, **6**, 53–75.
80 S. Chen, X. Chang, G. Sun, T. Zhang, Y. Xu, Y. Wang, C. Pei and J. Gong, *Chem. Soc. Rev.*, 2021, **50**, 3315–3354.
81 Q. Jiang, Z. Chen, J. Tong, M. Yang, Z. Jiang and C. Li, *ACS Catal.*, 2016, **6**, 1172–1180.
82 C. Li and G. Wang, *Chem. Soc. Rev.*, 2021, **50**, 4359–4381.
83 G. Deo and I. E. Wachs, *J. Catal.*, 1994, **146**, 323–334.
84 J. H. Blank, J. Beckers, P. F. Collignon and G. Rothenberg, *ChemPhysChem*, 2007, **8**, 2490–2497.
85 T. Blasco and J. M. L. Nieto, *Appl. Catal., A*, 1997, **157**, 117–142.
86 C. Zuo and Q. Su, *Molecules*, 2023, **28**, 3594.
87 S. Al-Ghamdi, J. Moreira and H. de Lasa, *Ind. Eng. Chem. Res.*, 2014, **53**, 15317–15332.
88 T. Wu, Q. Yu, L. Hou, W. Duan, K. Wang and Q. Qin, *J. Therm. Anal. Calorim.*, 2020, **140**, 1837–1843.
89 K. Fukudome, N.-o. Ikenaga, T. Miyake and T. Suzuki, *Catal. Sci. Technol.*, 2011, **1**, 987–998.

90 M. D. Argyle and C. H. Bartholomew, *Catalysts*, 2015, **5**(1), 145–269.
91 Y. Gao, F. Haeri, F. He and F. Li, *ACS Catal.*, 2018, **8**, 1757–1766.
92 A. Qiao, V. N. Kalevaru, J. Radnik and A. Martin, *Catal. Today*, 2016, **264**, 144–151.
93 Y. Wu, J. Gao, Y. He and T. Wu, *Appl. Surf. Sci.*, 2012, **258**, 4922–4928.
94 A. H. Elbadawi, M. S. Ba-Shammakh, S. Al-Ghamdi, S. A. Razzak, M. M. Hossain and H. I. de Lasa, *Chem. Eng. Res. Des.*, 2017, **117**, 733–745.
95 B. Xu, X. Zhu, Z. Cao, L. Yang and W. Yang, *Chin. J. Catal.*, 2015, **36**, 1060–1067.
96 F. Klose, T. Wolff, H. Lorenz, A. Seidel-Morgenstern, Y. Suchorski, M. Piórkowska and H. Weiss, *J. Catal.*, 2007, **247**, 176–193.
97 Z. Wu, H.-S. Kim, P. C. Stair, S. Rugmini and S. D. Jackson, *J. Phys. Chem. B*, 2005, **109**, 2793–2800.
98 J. M. L. Nieto, *Top. Catal.*, 2006, **41**, 3–15.
99 I. E. Wachs and B. M. Weckhuysen, *Appl. Catal., A*, 1997, **157**, 67–90.
100 A. Galli, J. M. López Nieto, A. Dejoz and M. I. Vazquez, *Catal. Lett.*, 1995, **34**, 51–58.
101 S. Al-Ghamdi, M. Volpe, M. M. Hossain and H. de Lasa, *Appl. Catal., A*, 2013, **450**, 120–130.
102 I. E. Wachs, J.-M. Jehng, G. Deo, B. M. Weckhuysen, V. V. Guliants and J. B. Benziger, *Catal. Today*, 1996, **32**, 47–55.
103 B. M. Weckhuysen and D. E. Keller, *Catal. Today*, 2003, **78**, 25–46.
104 M. V. Martínez-Huerta, X. Gao, H. Tian, I. E. Wachs, J. L. G. Fierro and M. A. Bañares, *Catal. Today*, 2006, **118**, 279–287.
105 K. Chen, A. T. Bell and E. Iglesia, *J. Catal.*, 2002, **209**, 35–42.
106 A. A. Lemonidou, L. Nalbandian and I. A. Vasalos, *Catal. Today*, 2000, **61**, 333–341.
107 A. J. Al Abdulghani, U. Kurumbail, S. Dong, N. R. Altvater, R. W. Dorn, M. C. Cendejas, W. P. McDermott, T. O. Agbi, C. M. Queen, M. Alvear, A. R. Head, A. J. Rossini and I. Hermans, *ACS Catal.*, 2025, **15**, 5557–5567.
108 F. J. Passamonti, S. A. D'Ippolito, M. A. Vicerich, M. A. Sanchez, S. Bocanegra, N. Guignard, C. Especel, F. Epron, C. L. Pieck and V. M. Benítez, *Ind. Eng. Chem. Res.*, 2025, **64**, 1021–1031.
109 M. Mandal, M. R. Hermes, F. Berger, J. Sauer and L. Gagliardi, *J. Phys. Chem. C*, 2025, **129**(32), 14418–14429.
110 J. A. M. Mesa, M. Shah, M. G. Rigamonti, P. Eloy, D. P. Debecker, I. A. Khan, I. Khalil and M. Dusselier, *Catal. Sci. Technol.*, 2025, 5295–5317.
111 Q. Liu, J. Li, Z. Zhao, M. Gao, L. Kong, J. Liu and Y. Wei, *Catal. Sci. Technol.*, 2016, **6**, 5927–5941.
112 X. Rozanska, R. Fortrie and J. Sauer, *J. Am. Chem. Soc.*, 2014, **136**, 7751–7761.
113 A. A. Ayandiran, I. A. Bakare, H. Binous, S. Al-Ghamdi, S. A. Razzak and M. M. Hossain, *Catal. Sci. Technol.*, 2016, **6**, 5154–5167.
114 P. Kandasamy, S. Gawali, A. T. Venugopalan, M. Manikandan, S. P. Mekala, A. Shelke, T. G. Ajithkumar, K. Bhatte and T. Raja, *New J. Chem.*, 2024, **48**, 15077–15087.
115 M. Fattahi, M. Kazemeini, F. Khorasheh and A. M. Rashidi, *Ind. Eng. Chem. Res.*, 2013, **52**, 16128–16141.
116 S. Rostom and H. de Lasa, *Ind. Eng. Chem. Res.*, 2018, **57**, 10251–10260.
117 I. A. Bakare, S. Adamu, M. Qamaruddin, S. A. Al-Bogami, S. Al-Ghamdi and M. M. Hossain, *Ind. Eng. Chem. Res.*, 2019, **58**, 10785–10792.
118 A. Benzaouak, H. Mahir, A. El Hamidi, M. Kacimi and L. F. Liotta, *Catalysts*, 2022, **12**(8), 811.
119 L. Schumacher, M. Funke and C. Hess, *RSC Sustainability*, 2024, **2**, 3846–3865.
120 A. Farzaneh and M. S. Moghaddam, *J. Colloid Interface Sci.*, 2023, **629**, 404–416.
121 X. Jiang, X. Zhang, S. C. Purdy, Y. He, Z. Huang, R. You, Z. Wei, H. M. Meyer, III, J. Yang, Y. Pan, P. Wu, W. Zhu, M. Chi, K. Page, W. Huang and Z. Wu, *JACS Au*, 2022, **2**, 1096–1104.
122 L. Cheng, G. A. Ferguson, S. A. Zygmunt and L. A. Curtiss, *J. Catal.*, 2013, **302**, 31–36.
123 S. Tao, X. Luo and S. Xu, *New J. Chem.*, 2024, **48**, 13743–13751.
124 F. Qiang, T. Guo, M. Nie, Y. Liu, M. Wu and Q. Guo, *Catalysts*, 2023, **13**(5), 797.
125 M. Pretz, B. Fish, L. Luo and B. Stears, Shaping the future of on-purpose propylene production, *Hydrocarbon Processing*, 2017, **https://www.hydrocarbonprocessing.com/magazine/2017/april-2017/special-focus-petrochemical-developments/shaping-the-future-of-on-purpose-propylene-production**.
126 J. J. Sattler, J. Ruiz-Martinez, E. Santillan-Jimenez and B. M. Weckhuysen, *Chem. Rev.*, 2014, **114**, 10613–10653.